

## Analytical Modeling of MHD Flow between two Permeable Non-Coincident Rotating Disks Embedded in Porous Medium in Presence of Variable Thermal Conductivity

V.G. Gupta<sup>1</sup> and Ajay Jain<sup>2</sup><sup>1</sup>Department of Mathematics, University of Rajasthan, Jaipur- 302004, Rajasthan.<sup>2</sup>Department of Mathematics, Regional College for Education, Research and Technology, Sitapura, Jaipur-302022, Rajasthan, India.

### ARTICLE INFO

#### Article history:

Received: 29 July 2017;

Received in revised form:

20 August 2017;

Accepted: 6 September 2017;

#### Keywords

MHD flow,  
Non-Coincident Disks,  
Porous Medium,  
Rotation.

### ABSTRACT

Modeling of steady magnetohydrodynamic viscous incompressible fluid flow through a porous medium between two disks rotating with same angular velocity about two non-coincident axes has been discussed taking into account the injection/suction, radiation and temperature dependent variable thermal conductivity. An exact solution of the governing equations has been obtained in a closed form by using perturbation along with dsolve Mat lab software tool to attain an analytical result for the velocity and the temperature profile. Analysis of the flow characteristics has been performed graphically by varying Hartmann number ( $M$ ), injection /suction parameter ( $\lambda$ ), permeability parameter ( $k_p$ ), rotation parameter ( $\Omega$ ), Prandtl number ( $p_r$ ), radiation parameter ( $M$ ) and the variable thermal conductivity ( $\epsilon$ ). The Skin friction coefficients are presented in pictorial from (11) to (15), and discussed in detail.

© 2017 Elixir All rights reserved.

### Introduction

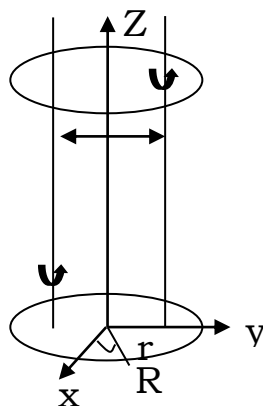


Fig. 1(a). Geometry of the problem.

Hydromagnetic viscous incompressible fluid flow through a porous medium has been the subject of intensive studies in recent years because of its wide applications in engineering and scientific technology such as in the petroleum technology to study the movement of natural gas, oil and water through the oil reservoirs, filtration and purification process etc.. The study of viscous flow near stationary or rotating discs has significant relevance to many applications for industrial devices. Many important applications have motivated studies involving complex geometries often with flow and heat transfer, for example, cooling a gas turbine, turbo machinery, boundary layer control, cooling of turbine blades, cooling the skins of high speed aircraft designs, computer disk drives and gas turbine rotors etc.. Further, the flow and heat transfer in any electrically conducting fluid flow system may be controlled by the application of an external magnetic field. Probably for the first time, the flow due to an infinite plane disk, rotating with constant angular velocity was discussed by Karman [1], Cochran [2] integrated numerically the equations obtained by Karman and compared his results with that of Karman.

Batchelor [3] and Stewartson [4] applied these equations to the problem of steady flow between two finite parallel plane discs, rotating at a finite distance apart. The flow due to a rotating disk of infinite radius with uniform suction at the disc has been discussed by Stuart [5]. Sparrow and Gregg [6] carried out the steady state heat transfer from a rotating disk maintained at a constant temperature to fluids at Prandtl number. Steady viscous flow between two rotating naturally permeable discs had been discussed by Chauhan and Gupta [7]. In the recent few years, it is generally admitted that the force due to the earth's rotation has a strong effect on the hydromagnetic flow in the earth's liquid core. MHD boundary layer flow is of great significance in understanding a variety of geophysical, astrophysical, and engineering problems that takes place at the core-mantle interface of the earth. Purohit and Bansal [8] considered the MHD flow of a viscous incompressible electrically conducting fluid between a rotating and a stationary naturally permeable disk. Due to the many applications of rotating disk flows with magnetic field, many researchers Ariel [9] Turkyilmazoglu [10] and Anjali Devi and Uma Devi [11] reported results on MHD rotating disk flow with various flows conditions and configurations. The flow of a viscous incompressible fluid confined between two parallel rotating with same angular velocity about non-coaxial axis explained by Berker [12] and Abott and Walters [13]. Erdogan [14, 15] worked on the flow due to parallel disks rotating about non-coincident axis with one of the disk or both the disks oscillating in its own plane. Mohanty [16] investigated the hydromagnetic flow between two rotating disks with non-coincident parallel axis of rotation. Kanch and Jana [17] explored the Hall effects on hydromagnetic flow between two rotating disk with non-coincident parallel axis of rotation. Maji et al. [18] explained the effect of rotation on unsteady MHD flow between disks, rotating with same angular velocity about two different axes. Das et al. [19] showed the Hall current on unsteady MHD flow between disks with non-coincident parallel axis of rotation. Jana et al. [20] discussed the effect of permeability and rotation on hydrodynamic flow between two non-coincident rotating disks. Srivastava [21] analyzed MHD flow of the micro polar fluid between eccentrically rotating disks.

The present work studies the effect of porosity, injection/suction on MHD flow of fluid between two permeable rotating disks with same angular velocity about two different axes at a distance  $d$  apart. Important aspects of variable thermal conductivity, thermal radiation effects are taken in consideration. The impact of dimensionless parameters on the velocity, temperature, skin friction coefficient is examined through the plots.

### Mathematical Analysis

We consider the steady MHD flow of an incompressible, viscous and electrically conducting fluid passes between two permeable parallel disks embedded in a porous medium rotating with uniform angular velocity  $\Omega$  about two different axis at a distance  $a$  apart. Let, the disks are in  $x, y$  plane and  $z$  axis is normal to it. The applied magnetic field  $\mathbf{B}_0$  along the  $z$  axis in the presence of constant injection /suction velocity  $\mathbf{w}_0$  is at one lower disk  $z=0$ . The electrical field owing to the polarization of charges and Hall current is taken negligible. The axis of rotation of the disk  $z=h$  lies to the right and that of the disk  $z=0$  lies to the left of the  $z$  axis and the  $z$  axis is taken middle of both of the disks. We choose a system of cylindrical polar coordinates  $(r, \theta, z)$  with axis normal to disk as situated symmetrically between two axis of rotation. Under these assumptions, the continuity, momentum and energy equations are governed by the following.

(a) Equation of continuity

$$\frac{\partial u}{\partial r} + \frac{u}{r} + \frac{\partial w}{\partial z} + \frac{1}{r} \frac{\partial v}{\partial \theta} = 0 \quad (1)$$

(b) Equation of momentum

$$\mathbf{u} \frac{\partial u}{\partial r} + \mathbf{w} \frac{\partial u}{\partial z} + \frac{v}{r} \frac{\partial u}{\partial \theta} - \frac{v^2}{r} = -\frac{\partial p}{\rho \partial r} + \nu \left( \frac{\partial^2 u}{\partial r^2} + \frac{1}{r} \frac{\partial u}{\partial r} + \frac{1}{r^2} \frac{\partial^2 u}{\partial \theta^2} + \frac{\partial^2 u}{\partial z^2} - \frac{2}{r^2} \frac{\partial v}{\partial \theta} - \frac{u}{r^2} \right) - \frac{\sigma \beta_0^2 u}{\rho} - \frac{v}{K_p} \mathbf{u} \quad (2)$$

$$\mathbf{u} \frac{\partial v}{\partial r} + \frac{v}{r} \frac{\partial v}{\partial \theta} + \mathbf{w} \frac{\partial v}{\partial z} + \frac{uv}{r} = \nu \left( \frac{\partial^2 v}{\partial r^2} + \frac{1}{r} \frac{\partial v}{\partial r} + \frac{1}{r^2} \frac{\partial^2 v}{\partial \theta^2} + \frac{\partial^2 v}{\partial z^2} + \frac{2}{r^2} \frac{\partial u}{\partial \theta} - \frac{v}{r^2} \right) - \frac{\sigma \beta_0^2 u}{\rho} - \frac{v}{K_p} \mathbf{v} \quad (3)$$

$$\mathbf{u} \frac{\partial w}{\partial r} + \frac{v}{r} \frac{\partial w}{\partial \theta} + \mathbf{w} \frac{\partial w}{\partial z} = -\frac{\partial p}{\rho \partial z} + \nu \left( \frac{\partial^2 w}{\partial r^2} + \frac{1}{r} \frac{\partial w}{\partial r} + \frac{1}{r^2} \frac{\partial^2 w}{\partial \theta^2} + \frac{\partial^2 w}{\partial z^2} \right) - \frac{v}{K_p} \quad (4)$$

Where,  $\mathbf{u}, \mathbf{v}, \mathbf{w}_0$  (constant) is the velocity in the direction of  $\mathbf{r}, \theta$  and  $\mathbf{z}$  respectively. The parameters,  $p, \rho, \nu$ , and  $\bar{k}_p$  are the fluid pressure, density of the fluid, the fluid kinematic viscosity and the permeability of the porous medium respectively.

(c) Equation of Energy

$$\rho c_p \left( \mathbf{u} \frac{\partial \bar{\theta}}{\partial r} + \mathbf{w}_0 \frac{\partial \bar{\theta}}{\partial z} \right) - \frac{\partial}{\partial r} \left( \bar{k} \frac{\partial \bar{\theta}}{\partial r} \right) + \bar{k} \left( \frac{\partial \bar{\theta}}{\partial r} \right) + \frac{\partial}{\partial z} \left( \bar{k} \frac{\partial \bar{\theta}}{\partial z} \right) - \frac{\partial q_1}{\partial z} = 0 \quad (5)$$

Where,

$$\frac{\partial q_1}{\partial z} = 4\alpha_1^2 (\bar{\theta} - \theta_w) \quad (6)$$

The corresponding boundary conditions are

$$\begin{aligned} \mathbf{u} &= -\frac{1}{2} \Omega a \cos \theta, \mathbf{v} = \Omega \left( r + \frac{1}{2} a \sin \theta \right), \mathbf{w} = \mathbf{w}_0, \bar{\theta} = \theta_0 \text{ at } \mathbf{z} = 0 \\ \mathbf{u} &= \frac{1}{2} \Omega a \cos \theta, \mathbf{v} = \Omega \left( r - \frac{1}{2} a \sin \theta \right), \mathbf{w} = 0, \bar{\theta} = \theta_w \text{ at } \mathbf{z} = h \end{aligned} \quad (7)$$

We assume the velocity components according to above boundaries expression as

$$\begin{aligned} \mathbf{u} &= \mathbf{A}(z) \cos \theta + \mathbf{B}(z) \sin \theta \\ \mathbf{v} &= \Omega \mathbf{r} + \mathbf{B}(z) \cos \theta - \mathbf{A}(z) \sin \theta \text{ and } \mathbf{w} = \mathbf{w}_0 \end{aligned} \quad (8)$$

Using the above assumption, the equations (2), (3) and (4) become

$$w_0(A'(z) \cos\theta + B'(z) \sin\theta) - \Omega^2 r - \Omega(B(z) \cos\theta - A(z) \sin\theta) = -\frac{\partial p}{\rho \partial r} + v(A''(z) \cos\theta + B''(z) \sin\theta) - \frac{\sigma\beta_0^2}{\rho}(A(z) \cos\theta + B(z) \sin\theta) - \frac{v}{K_p}(A(z) \cos\theta + B(z) \sin\theta) \quad (9)$$

$$w_0(-A'(z) \sin\theta + B'(z) \cos\theta) + \Omega(A(z) \sin\theta + B(z) \cos\theta) = v(B''(z) \cos\theta - A''(z) \sin\theta) - \frac{\sigma\beta_0^2}{\rho}(\Omega r + B(z) \cos\theta - A(z) \sin\theta) - \frac{v}{K_p}(\Omega r + B(z) \cos\theta - A(z) \sin\theta) \quad (10)$$

$$-\frac{\partial p}{\rho \partial z} - \frac{v}{K_p} w_0 = 0 \quad (11)$$

Where, prime denotes differentiation **w. r. t. z**

Eliminating **p** from the equation (9) - (11), we get

$$w_0(A''(z) \cos\theta + B''(z) \sin\theta) - \Omega(B'(z) \cos\theta - A'(z) \sin\theta) = v(A'''(z) \cos\theta + B'''(z) \sin\theta) - \frac{\sigma\beta_0^2}{\rho}(A'(z) \cos\theta + B'(z) \sin\theta) - \frac{v}{K_p}(A'(z) \cos\theta + B'(z) \sin\theta) \quad (12)$$

$$w_0(-A''(z) \sin\theta + B''(z) \cos\theta) + \Omega(A'(z) \cos\theta + B'(z) \sin\theta) = v(B'''(z) \cos\theta - A'''(z) \sin\theta) - \frac{\sigma\beta_0^2}{\rho}(B'(z) \cos\theta - A'(z) \sin\theta) - \frac{v}{K_p}(B'(z) \cos\theta - A'(z) \sin\theta) \quad (13)$$

$$-\frac{\partial^2 p}{\rho \partial z^2} = 0 \quad (14)$$

This implies,

$$-w_0 \frac{d^2 A}{dz^2} + v \frac{d^3 A}{dz^3} + \Omega \frac{dB}{dz} - \frac{\sigma\beta_0^2}{\rho} \frac{dA}{dz} - \frac{v}{K_p} \frac{dA}{dz} = 0 \quad (15)$$

$$-w_0 \frac{d^2 B}{dz^2} + v \frac{d^3 B}{dz^3} - \Omega \frac{dA}{dz} - \frac{\sigma\beta_0^2}{\rho} \frac{dB}{dz} - \frac{v}{K_p} \frac{dB}{dz} = 0 \quad (16)$$

The boundary conditions from the equation (7) using the expression given in equation (8), we get

$$A = -\frac{1}{2} \Omega a, B=0, \text{ at } z = 0$$

$$A = \frac{1}{2} \Omega a, B=0, \text{ at } z = h \quad (17)$$

Now the equations (15), (16) and (5) can be written in a non-dimensional form as

$$-\lambda \frac{d^2 f}{d\eta^2} + \frac{d^3 f}{d\eta^3} + k^2 \frac{dg}{d\eta} - \left(M^2 + \frac{1}{k_p}\right) \frac{df}{d\eta} = 0 \quad (18)$$

$$-\lambda \frac{d^2 g}{d\eta^2} + \frac{d^3 g}{d\eta^3} - k^2 \frac{df}{d\eta} - \left(M^2 + \frac{1}{k_p}\right) \frac{dg}{d\eta} = 0 \quad (19)$$

$$p_r \lambda \frac{d\varphi}{d\eta} = \frac{d}{d\eta} \left( (1 + \varepsilon\varphi) \frac{d\varphi}{d\eta} \right) - R^2 \varphi \quad (20)$$

Where,

$$f(\eta) = \frac{A}{\Omega a}, g(\eta) = \frac{B}{\Omega a}, \eta = \frac{z}{h}, \varphi(\eta) = \frac{\bar{\theta} - \theta_w}{\theta_0 - \theta_w}, k^2 = \frac{\Omega h^2}{v} k_p = \frac{\bar{K}_p}{h^2}, M^2 = \frac{\sigma\beta_0^2}{\rho v} h^2, \lambda = \frac{w_0 h}{v}, p_r = \frac{\mu C_p}{K}, R^2 = 4h^2 \frac{\alpha_1^2}{k}$$

(Cogley et al. [22])

$k^2$  is the rotation parameter,  $M$  is the Hartmann number,  $k_p$  is the permeability parameter,  $\lambda$  the suction/ injection parameter,  $R^2$  is the thermal radiation,  $p_r$  is the Prandtl number,  $\alpha_1$  is the heat absorption parameter,  $\theta_0$  temperature of lower disk,  $\theta_w$  temperature of upper disk. Arunachalam and Rajappa [23] expressed the linear relation between thermal diffusivity and temperature as  $\bar{k} = k(1 + \varepsilon\varphi(\eta))$  where  $\varepsilon \ll 1$  is a parameter which depends on the nature of the fluid and  $k$  is the thermal diffusivity.  $\varphi$  is the dimensionless temperature of the of fluid at any point.

The corresponding boundaries

$$f = -\frac{1}{2}, g=0, \varphi = 1 \quad \text{at } \eta = 0$$

$$f = \frac{1}{2}, g=0, \varphi = 0 \quad \text{at } \eta=1 \quad (21)$$

#### Solution of the Problem

Integrating the above (18) and (19) **w. r. t.  $\eta$** , we get

$$-\lambda \frac{df}{d\eta} + \frac{d^2 f}{d\eta^2} + k^2 g - \left(M^2 + \frac{1}{k_p}\right) f = a_1 \quad (22)$$

$$-\lambda \frac{dg}{d\eta} + \frac{d^2 g}{d\eta^2} - k^2 f - \left(M^2 + \frac{1}{k_p}\right) g = a_2 \quad (23)$$

Now, we combining the equations (22) and (23), we get

$$-\lambda \frac{d\xi}{d\eta} + \frac{d^2\xi}{d\eta^2} - \left( M^2 + \frac{1}{k_p} + ik^2 \right) \xi = a_3 \quad (24)$$

Where,

$$\xi = f + ig, \quad a_3 = a_1 + ia_2,$$

The corresponding boundary conditions become

$$\begin{aligned} \xi &= -\frac{1}{2}, \quad \varphi=1, & \text{at } \eta=0 \\ \xi &= \frac{1}{2}, \quad \varphi=0, & \text{at } \eta=1 \end{aligned} \quad (25)$$

We may choose to symmetric flow i.e,  $a_3 = 0$  and the equation (24) become

$$-\lambda \frac{d\xi}{d\eta} + \frac{d^2\xi}{d\eta^2} - \left( M^2 + \frac{1}{k_p} + ik^2 \right) \xi = 0 \quad (26)$$

The solution of the equation (26) subject to boundary condition (25), can be found by using Mat Lab dsolve software tool in the following form

$$\xi = \frac{e^{\lambda\eta/2}}{\cosh 2\alpha - \cos 2\beta} \left[ e^{-\frac{\lambda}{2}} \{ \sinh \alpha \eta \cos \beta \eta + i \cosh \alpha \eta \sin \beta \eta \} + \{ \sinh \alpha (\eta - 1) \cos \beta (\eta - 1) + i \cosh \alpha (\eta - 1) \sin \beta (\eta - 1) \} \right] (\sinh \alpha \cos \beta - i \cosh \alpha \sin \beta) \quad (27)$$

Real part

$$\begin{aligned} f &= \frac{e^{\lambda\eta/2}}{\cosh 2\alpha - \cos 2\beta} \left[ e^{-\frac{\lambda}{2}} \{ (\sinh \alpha \eta \cos \beta \eta) \sinh \alpha \cos \beta + (\cosh \alpha \eta \sin \beta \eta) \cosh \alpha \sin \beta \} + \right. \\ &\quad \left. (\sinh \alpha (\eta - 1) \cos \beta (\eta - 1)) \sinh \alpha \cos \beta + (\cosh \alpha (\eta - 1) \sin \beta (\eta - 1)) \cosh \alpha \sin \beta \right]. \end{aligned} \quad (28)$$

Imaginary part

$$\begin{aligned} g &= \frac{e^{\lambda\eta/2}}{\cosh 2\alpha - \cos 2\beta} \left[ e^{-\frac{\lambda}{2}} \{ (-\sinh \alpha \eta \cos \beta \eta) \cosh \alpha \sin \beta + (\cosh \alpha \eta \sin \beta \eta) \sinh \alpha \cos \beta \} + \right. \\ &\quad \left. (-\sinh \alpha (\eta - 1) \cos \beta (\eta - 1)) \cosh \alpha \sin \beta + (\cosh \alpha (\eta - 1) \sin \beta (\eta - 1)) \sinh \alpha \cos \beta \right] \end{aligned} \quad (29)$$

Where,

$$\alpha = \frac{1}{\sqrt{2}} \left( \lambda_1 + \sqrt{\lambda_1^2 + k^4} \right)^{\frac{1}{2}}, \quad \beta = \frac{1}{\sqrt{2}} \left( -\lambda_1 + \sqrt{\lambda_1^2 + k^4} \right)^{\frac{1}{2}}, \quad \lambda_1 = \frac{\lambda^2}{4} + M^2 + \frac{1}{k_p}$$

Now, the solution of energy equation (20) subject to boundary condition (25) using regular perturbation technique along with dsolve Mat Lab software tool is

$$\varphi = \varphi_0 + \varepsilon \varphi_1 + O(\varepsilon^2) \quad (30)$$

Here,  $\varepsilon \ll 1$  the small variable thermal conductivity parameter.

$$\begin{aligned} \varphi_0 &= \frac{e^{m_2} e^{m_1 \eta} - e^{m_1} e^{m_2 \eta}}{e^{m_2} - e^{m_1}} \\ \varphi_1 &= c_3 e^{m_1 \eta} + c_4 e^{m_2 \eta} - \frac{A_1 e^{2m_1 \eta}}{4m_1^2 - 2p_r \lambda m_1 - R^2} - \frac{A_2 e^{(m_1 + m_2) \eta}}{(m_1 + m_2)^2 - p_r \lambda (m_1 + m_2) - R^2} - \frac{A_3 e^{2m_2 \eta}}{4m_2^2 - 2p_r \lambda m_2 - R^2} \end{aligned} \quad (31)$$

Constants are left for the sake of brevity.

#### (5.4) Skin Friction Coefficient

The shear stress or the Skin-friction due to primary and secondary velocity at the lower and upper disk can be found such as The shear stress due to primary velocity at the lower disk is

$$\begin{aligned} f'(\eta)_{\eta=0} &= \frac{1}{\cosh 2\alpha - \cos 2\beta} \left[ e^{-\frac{\lambda}{2}} (\alpha \sinh \alpha \cos \beta + \beta \cosh \alpha \sin \beta) + \right. \\ &\quad \left. (\alpha \cosh \alpha \cos \beta + \beta \sinh \alpha \sin \beta) \sinh \alpha \cos \beta + (\alpha \sinh \alpha \sin \beta + \beta \cosh \alpha \cos \beta) \cosh \alpha \sin \beta \right] + \\ &\quad \frac{\lambda}{2} \end{aligned} \quad (32)$$

The shear stress due to primary velocity at the upper disk is

$$f'(\eta)_{\eta=1} = \left[ \frac{e^{\lambda/2}}{\cosh 2\alpha - \cos 2\beta} \left[ e^{-\frac{\lambda}{2}} \{ (\alpha \cosh \alpha \cos \beta - \beta \sinh \alpha \sin \beta) \sinh \alpha \cos \beta + (\alpha \sinh \alpha \sin \beta + \beta \cosh \alpha \cos \beta) \cosh \alpha \sin \beta \} + \alpha \sinh \alpha \cos \beta + \beta \cosh \alpha \sin \beta \right] + \frac{\lambda}{2} \left( \frac{e^{\frac{\lambda}{2}}}{\cosh 2\alpha - \cos 2\beta} \right) \right] \quad (33)$$

The shear stress due to secondary velocity at the lower disk is

$$g'(\eta)_{\eta=0} = \frac{1}{\cosh 2\alpha - \cos 2\beta} \left[ e^{-\frac{\lambda}{2}} (-\alpha \cosh \alpha \sin \beta + \beta \sinh \alpha \cos \beta) + (\alpha \cosh \alpha \cos \beta - \beta \sinh \alpha \sin \beta) (-\cosh \alpha \sin \beta) + (\alpha \sinh \alpha \sin \beta + \beta \cosh \alpha \cos \beta) (\sinh \alpha \cos \beta) \right] + \frac{\lambda}{2} \frac{1}{(\cosh 2\alpha - \cos 2\beta)} \quad (34)$$

The shear stress due to secondary velocity at the lower disk is

$$g'(\eta)_{\eta=1} = \frac{e^{\frac{\lambda}{2}}}{\cosh 2\alpha - \cos 2\beta} \left[ e^{-\frac{\lambda}{2}} (-\alpha \cosh \alpha \cos \beta + \beta \sinh \alpha \sin \beta) \cosh \alpha \sin \beta + (\alpha \sinh \alpha \sin \beta + \beta \cosh \alpha \cos \beta) \sinh \alpha \cos \beta - \alpha \cosh \alpha \sin \beta + \beta \sinh \alpha \cos \beta \right] + \frac{\lambda}{2} \frac{e^{\frac{\lambda}{2}}}{(\cosh 2\alpha - \cos 2\beta)} \quad (35)$$

### Torque

The torque exerted by the fluid to control the transverse shearing stress on a disk of radius  $l$ , such as; Torque

$$= 2 \int_0^l \int_0^\pi f'(0) r^2 dr d\theta$$

### Result and Discussion

In order to have a physical insight of the problem, the variation of the velocity, temperature, Skin friction and torque are evaluated numerically for the different sets of values of suction /injection parameter  $\lambda$ , rotation parameter  $k^2$ , porosity parameter  $k_p$ , Magnetic parameter  $M$ , radiation parameter  $R^2$ , thermal conductivity parameter  $p_r$  (Prandtl number) and variable thermal conductivity  $\varepsilon$ . Further, it is assumed that the temperature difference is small enough so that the density changes of the fluid in the system will be small. When the injection/suction parameter  $\lambda$  is positive, fluid is injected through the hot disk at  $\eta = 0$  while suction phenomenon occurs in case of  $\lambda$  negative. The influence of various physical parameters on the velocity flow field (fig. 1-10), temperature distribution (fig. 18-21), Skin friction (fig. 11-15) and the torque (fig 16 (a)-17) are presented graphically and then analyzed in detail. We fix the value of parameters, namely,  $k^2=5$ ,  $M=.5$ ,  $k_p=.2$ ,  $\lambda=0.1$  for primary and secondary velocity profile, whereas  $\lambda=-1$ ,  $R=2$ ,  $p_r=7$ ,  $\varepsilon=0.1$  for a temperature distribution profile to assess the effect of changing each parameter one by one.

Taking  $M=0$  and  $\lambda=0$  in Figure (1) illustrates that the primary and secondary velocity  $f$  and  $g$  respectively, rise with an increase in rotation parameter  $k^2$  to the left of the z-axis and both of the velocities decrease with an increase in  $k^2$  to the right of the z-axis. Again, taking  $M=0$  and  $\lambda=0$  in Figure (2) displays that the primary velocity  $f$  decreases with an increase in  $k_p$  to the left of z axis and it increases with growing  $k_p$  to the right of z axis whereas the secondary velocity  $g$  increases with increasing  $k_p$  to the left of the z axis and it becomes reverse to the right of z axis. Both the figures have explained good agreement with the results and the figures of Jana et al. [20]. Figure (3) shows that the primary velocity  $f$  decreases with an increase in  $k_p$  to the left of the z-axis and it shows the opposite consequences to the right of z-axis. On the other hand, the secondary velocity  $g$  increases with an increase in  $k_p$  to the left of the z-axis and it becomes reverse to the right of the z-axis as shown in figure (7). Figure (4) displays that the primary velocity  $f$  increases with an increase in rotation parameter  $k^2$  to the left of the z-axis and it decreases with an increase in  $k^2$  to the right of the z-axis while the same consequence is observed in figure (8) for secondary velocity  $g$ . Figure (5) illustrates that the primary velocity  $f$  increases with an increase in Hartmann number  $M$  in the left of the z-axis and it decreases with an increase in  $M$  to the right of the z-axis whereas reverse consequence is observed in figure (9) for secondary velocity  $g$ . Figure (6) demonstrates that the primary velocity  $f$  decreases when increasing the injection parameter while by increasing the suction increases the primary velocity. Again, from figure (10), we get the reversal phenomenon in the case of secondary velocity in comparison to the figure (6). The influences of porosity parameter  $k_p$ , rotation parameter  $k^2$  and injection/suction  $\lambda$  on Skin friction coefficient against Hartman number  $M$  due to primary and secondary velocity at the lower and upper disks are depicted in figures from (11) to (15). The Skin friction coefficient ( $f'(0)$ ) increases at lower disk ( $\eta=0$ ) with increasing values of  $k^2$  or  $M$  due to primary velocity while it shows the decreasing impact with increasing  $k_p$  or  $\lambda$ . The Skin friction coefficient ( $g'(0)$ ) increases at the lower disk ( $\eta=0$ ) for increasing values of  $k_p$ ,  $k^2$  or  $\lambda$  due to secondary velocity, but it reduces due to growing  $M$ . Increasing values of  $k^2$  or  $M$  enhances the Skin friction coefficient ( $f'(1)$ ) at the upper disk ( $\eta=1$ )

due to primary velocity while the reverse effect shows for increasing value of  $k_p$ . The Skin friction ( $g'(1)$ ) increases with growing  $k_p$  or  $k^2$  at the upper disk ( $\eta=1$ ) due to the secondary velocity whereas reverse phenomenon occurs in case of  $M$ . The variation in torque against  $k$  with  $k_p$  and  $M$  at the disk  $\eta=0$  is shown in figures (16 a) to 17. It is seen from these figures that the torque on the disk increases with an increase in either  $M$  or rotation parameter  $k$  whereas reverses the effect by increasing  $k_p$ . Figure (18) reveals that injection/suction parameter  $\lambda$  is negative; fluid temperature is sucked out at lower hot plate. It is also observed in figure (18) that an increase in the negative value of suction  $\lambda$  falls the temperature of the flow at lower hot plate while reversal result is observed in case of injection  $\lambda$ . It is due to injecting hot fluid particles, the temperature of fluid increases. It is therefore, concluded that by increasing  $\lambda$  from a negative value to a positive value the temperature of the flow between rotating disks enhances. Figure (19) shows that an increase in variable thermal conductivity  $\epsilon$  increases the temperature of the fluid. From figure (20), it is observed that decreasing the Prandtl number ( $p_r$ ) increases the thermal conductivity and therefore, heat is able to diffuse away from the disk more swiftly than the higher value  $p_r$  resulting in high temperature profile. The effects of radiation parameters ( $R$ ) on the temperature distribution are demonstrated in figure (21). It is viewed that as the value of  $R$  decreases, the temperature profile increases. This result can be explained by the fact that a decrease in the Radiation parameter  $R$ , decreases in the Rosseland radiation absorption ( $\alpha_1$ ) at the disk ( $R$  is proportional to  $\alpha_1$ ). It is concluded that the divergence of radiative heat flux  $\frac{\partial q^1}{\partial z}$  increases as  $\alpha_1$  decreases and this means that the rate of radiative heat transferred to the fluid increases consequently, the fluid temperature increases.

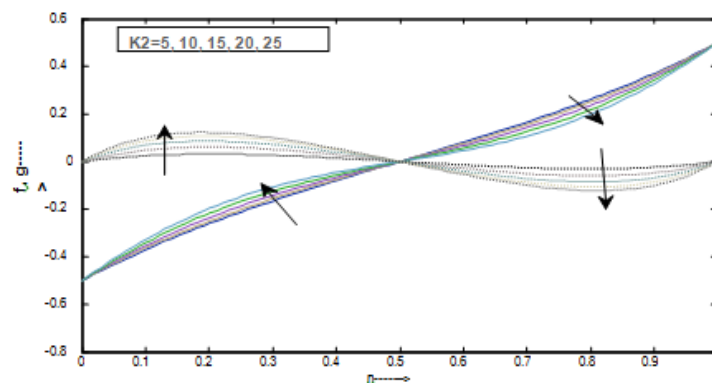


Fig. 1. variation of primary velocity f and secondary velocity g for  $K_p=0.2, M=0, \lambda=0$ .

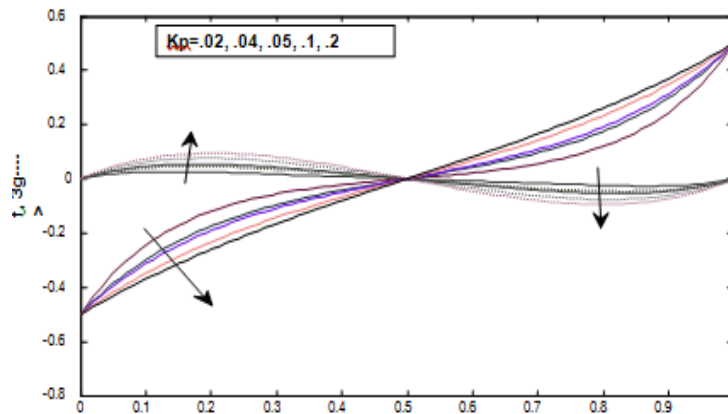


Fig. 2. Variations of primary velocity f and secondary velocity g for  $k_2=5, M=0, \lambda=0$ .

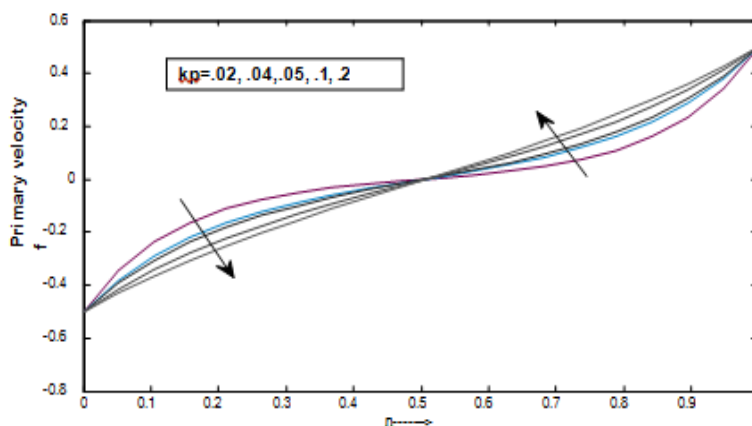


Fig.3. primary velocity against distance  $\eta$ .

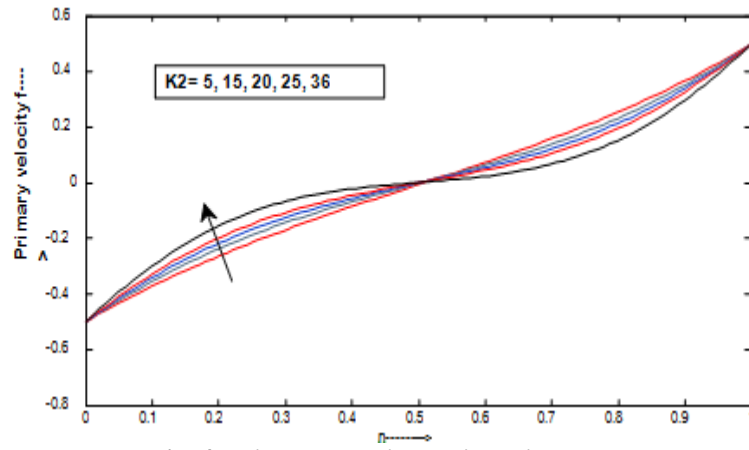


Fig. 4. primary velocity against distance  $\eta$ .

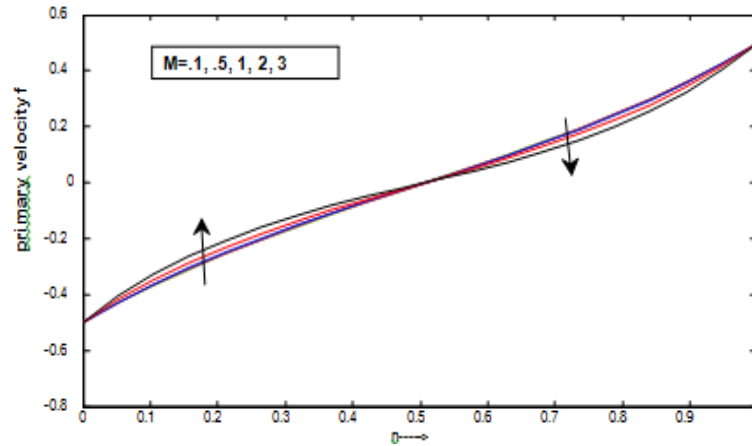


Fig. 5. primary velocity against distance  $\eta$ .

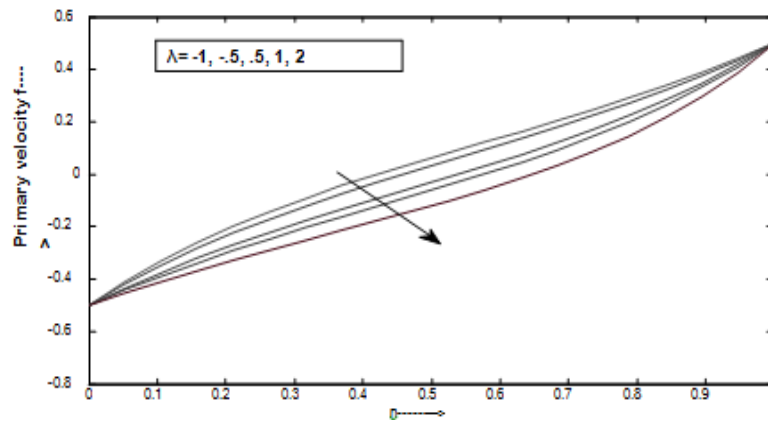


Fig. 6. primary velocity f against distance  $\eta$ .

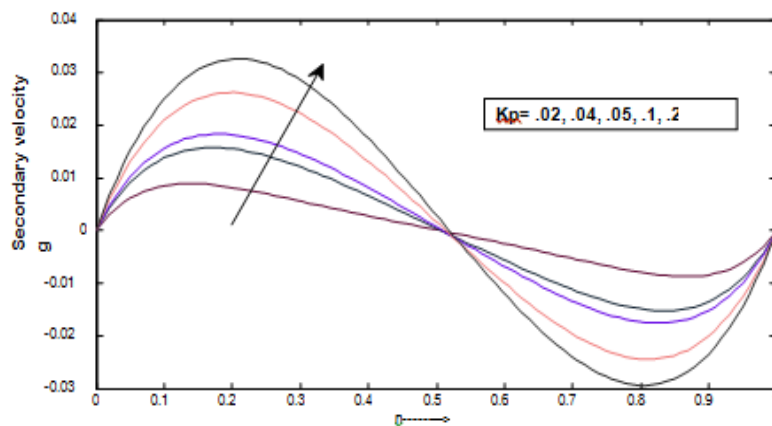


Fig. 7. Secondary velocity against distance  $\eta$ .

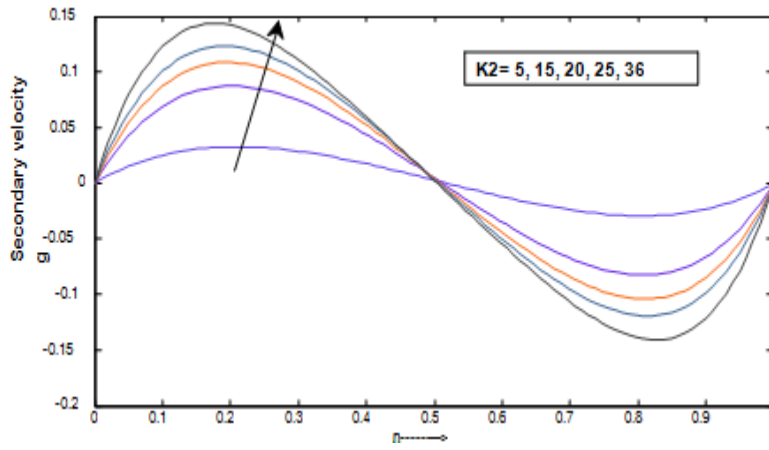


Fig. 8. secondary velocity against distance  $\eta$ .

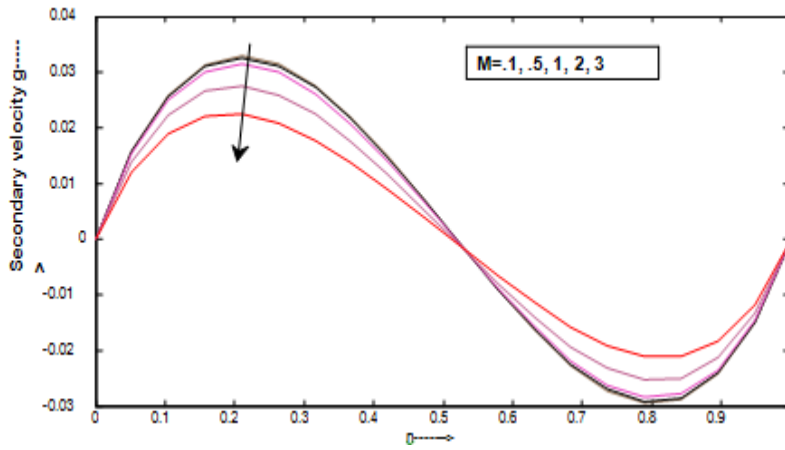


Fig. 9. Secondary velocity against distance  $\eta$ .

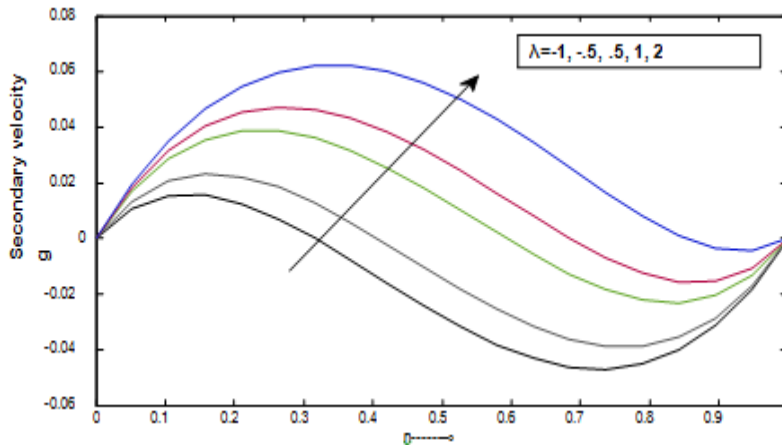


Fig. 10. secondary velocity against  $\eta$ .

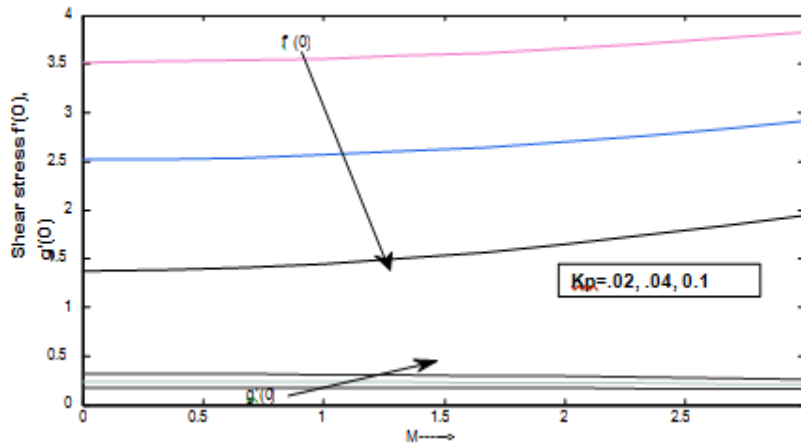


Fig. 11. shear stress against M at  $\eta = 0$ .

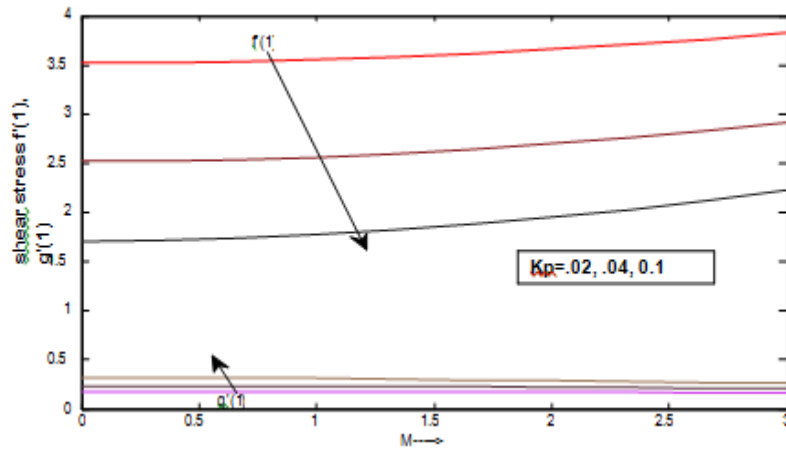


Fig. 12. shear stress at  $\eta = 1$ .

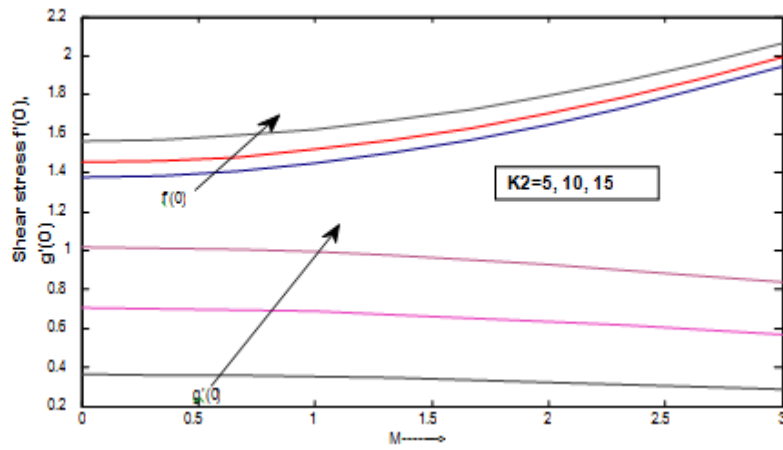


Fig.13. shear stress at  $\eta = 0$ .

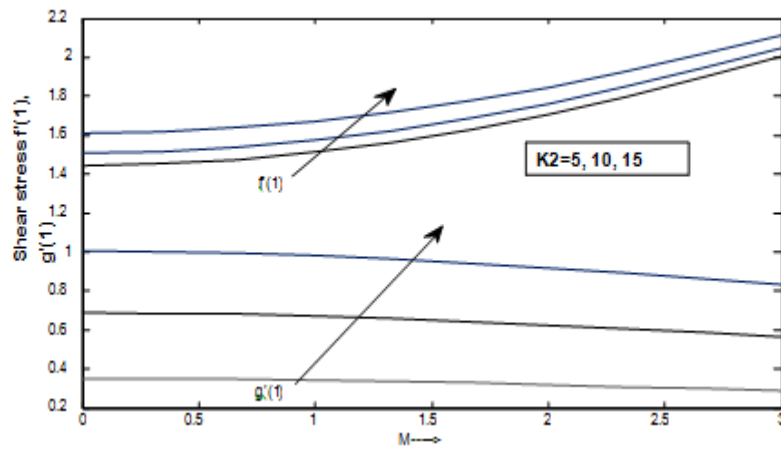


Fig.14. shear stress at  $\eta = 1$ .

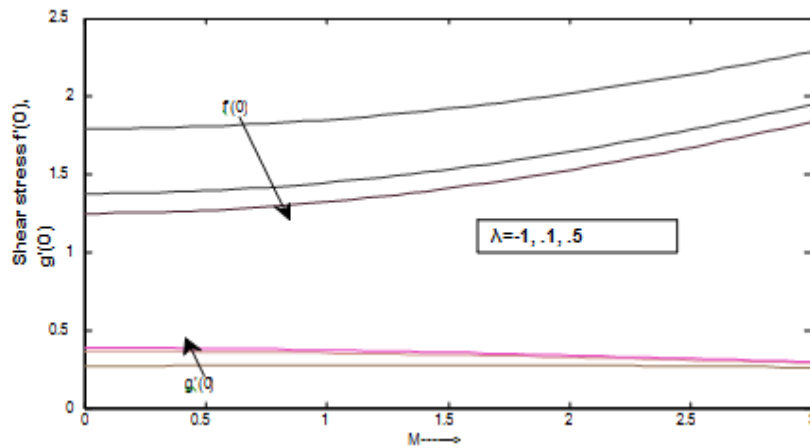


Fig. 15. shearstress at  $\eta = 0$ .

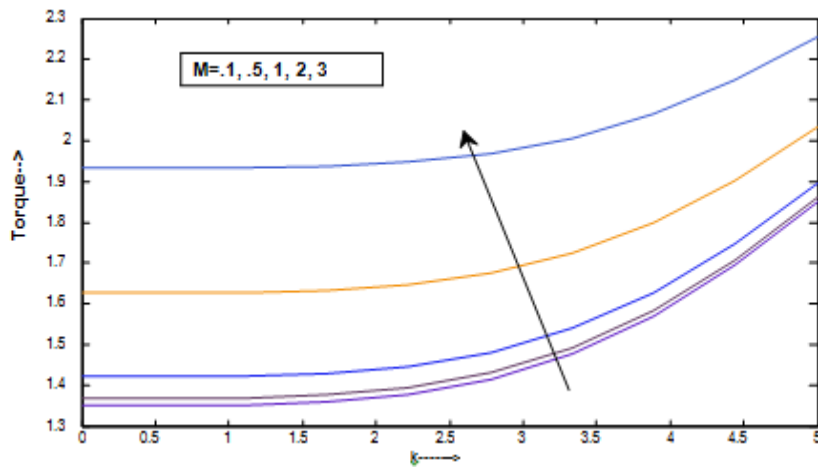


Fig. 16(a). Torque against rotation parameter k.

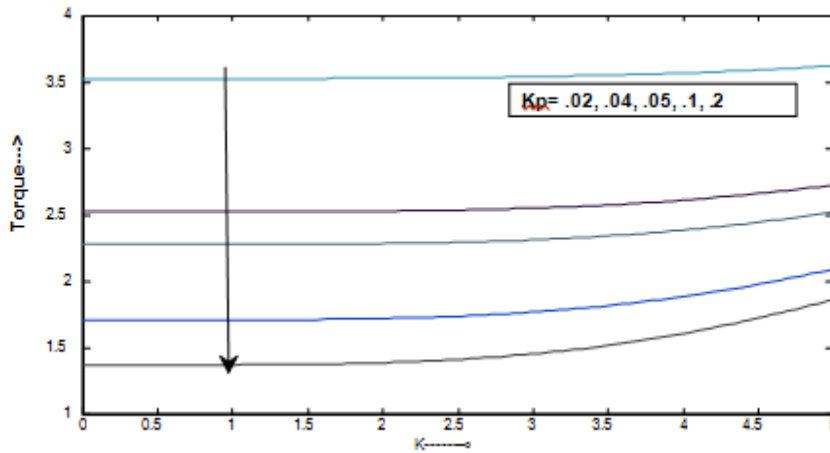


Fig. 17. Variation of Torque.

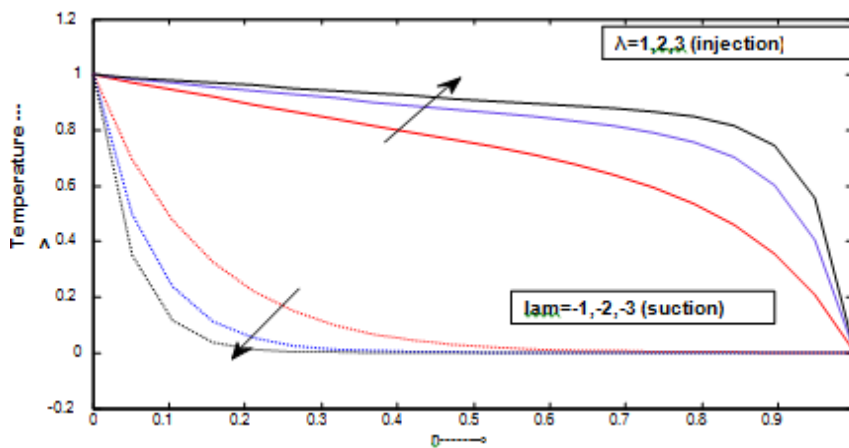


Fig 18. temperature against distance  $\eta$ .

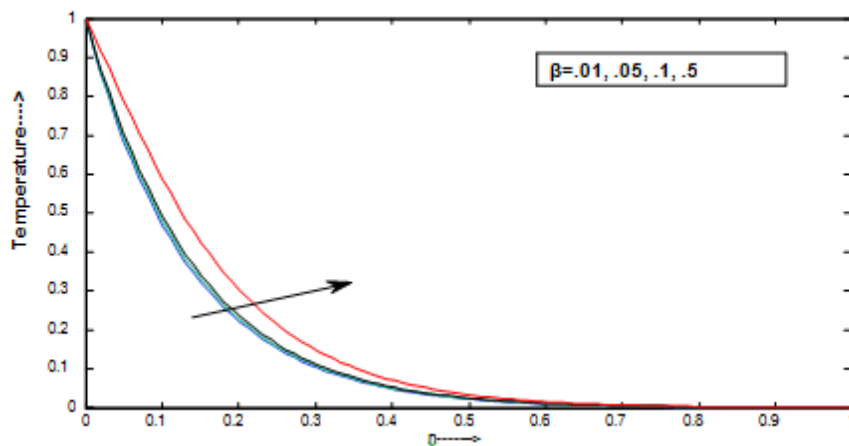
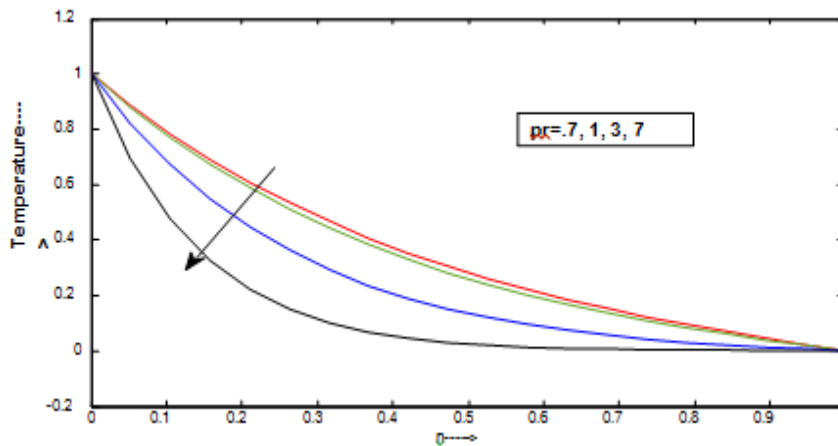
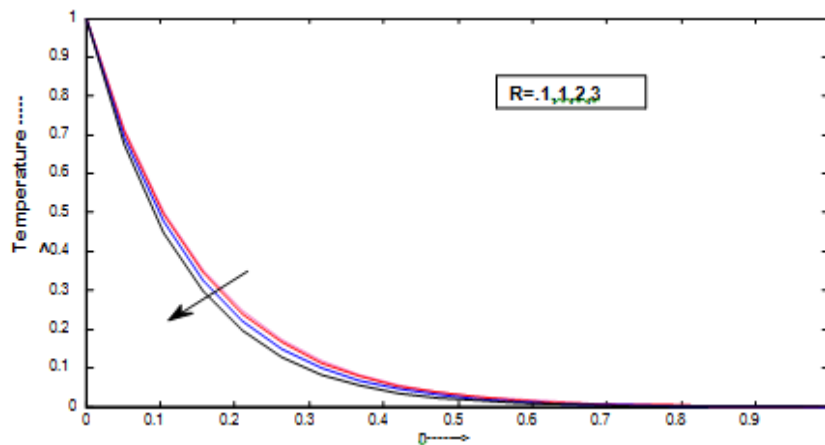


Fig 19. temperature against distance n.

Fig .20. temperature against distance  $\eta$ .Fig. 21. temperature against distance  $\eta$ .

### Conclusions

The following results are concluded.

It is explained that the primary velocity  $f$  increases with the increasing  $M$  or  $k^2$  to the left of the  $z$ - axis and the result is reversed to the right of  $z$  – axis whereas the growing  $k_p$  reverses the consequences. The secondary velocity  $g$  increases with the increase of  $k_p$  or  $k^2$  to the left of the  $z$  axis and the result is reversed to the right of  $z$  axis while growing  $M$  reverses the consequences. The primary velocity increases with increasing of suction ( $\lambda < 0$ ) while it is decreased by increasing the injection ( $\lambda > 0$ ). Again, the secondary velocity reverses the results for injection/suction in comparison to primary flow. The Skin-friction coefficient increases at lower disk with increasing  $k^2$  or  $M$  due to primary velocity while it shows the decreasing impact with increasing  $k_p$  or  $\lambda$ . The Skin-friction coefficient increases at the lower disk with the increase of  $k_p$ ,  $k^2$  or  $\lambda$  due to secondary velocity while an increase in  $M$  reduces the Skin-friction. With increasing  $k^2$  or  $M$  enhances the Skin-friction coefficient at upper disk due to primary velocity while the reverse effect shows by increasing  $k_p$ . The Skin-friction coefficient increases at the upper disk with growing  $k_p$ ,  $k^2$  due to the secondary velocity while the reverse phenomenon occurs in case of  $M$ . It is found that with increasing  $R$ ,  $p_r$  or  $\lambda < 0$  (at lower hot disk  $\eta = 0$ ) decreases the temperature of fluid, but reversal phenomenon occurs by growing  $\epsilon$  or ( $\lambda > 0$ ).

### References

1. Karman, T.V. (1921) Uber laminare and turbulente reibung, ZAMM, 1, 233-252.
2. Cochran, W.G. (1934) The flow due to a rotating disk, Proc. Camb. Phil. Soc., 30, 365-375.
3. Batchelor, G. K. (1951) Note on a class of solution of the Navier-Stokes equations representing steady non-rotationally symmetrical flow, Q. J. Mech. Appl. Math. 4, 29-41.
4. Stewartson, K. (1953) On the flow between two rotating coaxial disks, Proc. Camb. Phil. Soc., 49, 333-341.
5. Stuart J. T. (1954) On the effects of uniform suction on the steady flow due to a rotating disk, Q. J. Mech. Appl. Math., 7, 446-457.
6. Sparrow, E. M. and Gregg, J. L. (1960) Mass transfer flow and heat transfer about a rotating disk, Journal of Heat transfer, 82(4), 294-302.
7. Chauhan, D. S. and Gupta, S. (1999) Steady viscous flow between two rotating naturally permeable disks, Ganita Sandesh, 13(2), 53-64.
8. Purohit, G.N. and Bansal P. (1995) MHD flow between a rotating and a stationary naturally permeable porous discs, Ganita Sandesh, 9(2), 55-64.
9. Ariel, P. Donald (2009) The homotopy perturbation method and analytical solution of the problem of flow past a rotating disk,

Computers and Mathematic with Applications, 58(11), 2504-2513.

10. Turkyilmazoglu, M. (2011) Exact solutions for the incompressible viscous magnetohydrodynamic fluid of a rotating disk flow, International Journal of Non-Linear Mechanics, 46(1), 306-311.

11. Devi, Anjali and Devi, Uma (2011) On hydromagnetic flow due to a rotating disk with radiation effect, Nonlinear Analysis: Modelling and Control, 16(1), 17-29.

12. Berker, R. (1963) Hand Book of Fluid Dyanmics, VIII/3, Springer, Berlin.

13. Abott, T. N. G. and Walters, K. (1970) Rheometrical flow systems, Part. Theory for Orthogonal Rheometer, Including an Exact Solution of the Navier-Stokes Equations, Journal of Fluid Mechanics, 40,205-213.

14. Erdogan, M. E. (2000) Unsteady flow between eccentric rotating disks executing non-torsional oscillations, International journal of Non-Linear Mechanics, 35(4), 691-699.

15. Erdogan, M. E. (1995) Unsteady viscous flow between eccentric rotating disks, International journal of Non-Linear Mechanics, 30(5), 711-717.

16. Mohanty, H. K. (1972) Hydromagnetic flow between two rotating disks with non-coincident parallel axes of rotation, Physics of Fluids, 15(8), 1456-1458.

17. Kanch, A. K. and Jana R. N. (1992) Hall effects on hydromagnetic flow between two disks with non-coincident parallel axes of rotation, Revue Roumaine des Sciences Techniques,- Serie de Mecanique Appliquee, 37(4), 379-385.

18. Maji, S.L., Ghara, N., Jana, R. N., Das, S. (2009) Unsteady MHD flow between two eccentric rotating disks, Journal Physical Sciences, 13. 87-97.

19. Das. S., Maji, S. L., Guria, M. Jana, R. N. (2010) Hall effects on unsteady MHD flow between two disks with Non- Coincident Parallel axes of rotation, International Journal of Applied Mechanics and Engineering, 15(1), 5-18.

20. Jana, Ravindranath, Maji, Mrinal, Das, Sanatan, Maji, Sovan Lal, Ghosh Swapan Kumar (2011) Hydrpdynamic flow between two non-coincident rotating disks embedded in porous media, World Journal of Mechanics, 1, 50-56.

21. Srivastava, Neetu (2014) MHD flow of the micropolar fluid between eccentrically rotating disks, Hindawi Publishing Corporation, <http://dx.doi.org/10.1155/2014/317075>.

22. Cogley, A.C., Vincenti, W.C. and Gilles, S. E. (1968) Differential approximation for radiation transfer in a non gray gas near equilibrium, American Institute of Aeronautics and Astronautics Journal, 6, 551-555.

23. Arunachalam, M. and Rajappa, N. R. (1978) Forced convection in liquid metals with variable thermal conductivity and capacity, Acta Mechanica 31, 25-31